Sādhanā (2022)47:96
https://doi.org/10.1007/s12046-022-01862-x

Convective heat transfer in electromagnetohydrodynamic flow of third grade fluids through large parallel plates: a study on effect of parametric variation on thermal characteristics

SUMANTA CHAUDHURI, RAJIVA LOCHAN MOHANTY* and VIJAY KUMAR MISHRA

School of Mechanical Engineering, KIIT Deemed to be University, Bhubaneswar, Odisha 751024, India
e-mail: rajivamohanty@gmail.com

MS received 2 September 2021; revised 30 January 2022; accepted 24 February 2022

Abstract. Electromagnetohydrodynamic flow and heat transfer of a non-Newtonian third grade fluid through two parallel plates of large width are studied for both heating and cooling. The plates are subjected to uniform heat fluxes. A magnetic field and an electric field are externally imposed. The effects of viscous dissipation and Joule heating are included in the analysis. The non-linear equations governing the physical situation are solved by employing the Least Square Method (LSM), a semi-analytical technique widely applied for solving non-linear problems. For implementing the least square method, the presence of any small parameter is not required. Non-dimensional velocity and temperature distributions are obtained and the effects of the third grade fluid parameters, Hartmann number, electric field parameter, Brinkman number on the velocity, temperature, and Nusselt number are discussed. The results imply that the Nusselt number reverses its sign when the Brinkmann number reaches a critical value. The bulk mean temperature decreases so much that the difference between the wall temperature and the bulk mean temperature becomes negative, which results in a negative Nusselt number (indicating heat transfer from the fluid). In the case of heating, the Nusselt number increases with the Hartmann number for all values of the third grade fluid parameter.

Keywords. Electromagnetohydrodynamics; third grade fluid; Hartmann number; Brinkman number; least square method; Joule heating.

1. Introduction

The study of the interaction between a magnetic field and an electrically conducting fluid is termed "magnetohydrodynamics" (MHD). Many naturally occurring and man-made flows are governed by magnetic fields. Natural MHD flows are examples of natural fluid motion in the core of the earth, which maintains the terrestrial magnetic field. Sunspots generated by the solar magnetic field are examples of natural MHD flows. Natural MHD flows include the terrestrial magnetic field, which is maintained by fluid motion in the earth's core, as well as sun spots and solar flares generated by the solar magnetic field. In industrial applications, magnetic fields are widely used to transport, heat, and stir fluids. In MHD flow, the generation of the Lorentz force due to the interaction of the electrically conducting fluid and magnetic field is the key factor that provides a non-intrusive means for exercising better control over the liquid metal flows. The researchers have widely explored the MHD flows of engineering interest.

Over the last decade, the prospect of a technological shift toward miniaturisation has resulted in massive research in the fields of micro- and nano-scale flow and heat transfer. The flow of fluid in these micro-scale geometries is actuated by employing the electric field, magnetic field, or their appropriate combination. At the beginning, pressure gradient was employed to actuate the flow, but soon it was realised that the conventional pressure-induced flow had some serious detrimental effects like considerable power loss due to friction, reconfigurability with small scale devices, etc., which are reported in the study of Chakraborty *et al* [1]. These serious limitations of the conventional flow actuating mechanism have led to the application of the magnetic field, electric field, and their suitable combination. Among these, electromagnetohydrodynamic (EMHD) convection has attracted researchers because of its importance in the fields of biomedical processes, biochemical processes, heat exchangers, etc. Some important studies related to this are the investigations of Stone *et al* [2] and Ohono *et al* [3]. It is important to mention here that though EMHD flow does not suffer from the drawbacks associated with the conventional pressure gradient flow actuating mechanism, a suitable combination of the pressure gradient

*For correspondence
Published online: 03 May 2022

and EMHD ensures the efficient functioning of the majority of the microscale devices, as reported in the investigation by Chakraborty *et al* [1]. Since the inception of EMHD, numerous research works, both experimental and theoretical, have been published in the open literature.The conception of the EMHD micropump was first put forward by Jang and Lee [4]. Wang *et al* [5] carried out a numerical simulation of the two-dimensional laminar, fully developed flow of an MHD micropump. Ho [6] analysed the flow through a rectangular duct of an EMHD micropump. Rivero and Cuevas [7] investigated the flow characteristics of one and two-dimensional flows in an EMHD micropump under the influence of wall slip, as wall slip plays an important role in micro/nano-scale flow and heat transfer. In most cases, the real channels are not smooth and have roughness incurred on the wall surface during the fabrication process. Microchannel EMHD flow through corrugated walls was investigated analytically by Buren *et al* [8] and Buren and Jian [9] applying the perturbation method. The roughness of the upper and lower walls was approximated as small-amplitude sinusoidal waves, and by introducing a suitable perturbation parameter, an analytical solution was obtained.

In all the works cited above, the fluid involved was assumed to follow the Newtonian model. However, it is a well-established fact that many of the fluids utilised for applications in industries do not follow the linear stress-strain rate behaviour of the Newtonian model and are categorised as non-Newtonian fluids. The mentioned studies on MHD flow and heat transfer involved electrically conducting liquids. Numerous researchers have investigated the effect of the magnetic field on some electrically conducting non-Newtonian fluids too. As mentioned by Nayak *et al* [10], electrically conducting polymeric liquid can play an important role in polymer technology and the extrusion process. Nayak *et al* [10] investigated MHD flow and heat transfer of a non-Newtonian third grade fluid in the analysis of wire coating. Liu [11] investigated an electrically conducting second grade fluid under the influence of a magnetic field, flowing past a stretching sheet. The MHD slip flows of non-Newtonian second grade fluid and Walter's liquid B were investigated by Turkyilmazoglu [12]. The influence of the slip factor on the flow involving third grade fluids between the concentric cylinders was studied analytically by Ellahi *et al* [13]. The effects of pressure-gradient, non-Newtonian parameters, etc. on the velocity were discussed. Numerous problems of practical interest involving third grade fluids were investigated by numerous researchers [14–17]. In a recent paper, Zhang *et al* [16] studied the EMHD flow of third grade fluid through parallel plates filled with porous medium. A non-linear differential transform method (DTM) was used to solve the non-linear governing differential equation. The effects of various parameters on the flow and heat transfer characteristics were discussed. Wang *et al* [18] studied the EMHD flow and heat transfer of a third-grade fluid through parallel plates. The effects of viscous dissipation and Joule heating were considered, and analytical solutions for velocity and temperature were obtained. The Hartmann number, third grade fluid parameter, and Brinkman number were used to investigate heat transfer.Entropy generation evaluation and its minimization are important aspects in many situations, these aspects have been studied by numerous researchers [19–24].

Motivated by the above studies, EMHD heat transfer of a third grade fluid occurring between two large parallel plates has been undertaken. The walls of the plates are deferentially heated and subjected to constant and uniform heat fluxes. The effects of Joule heating and viscous dissipation are considered in the present investigation. Viscous dissipation can play a vital role in the thermal transport and thermal management of various engineering systems, especially in high viscous and high velocity flow phenomena. In the study by Wang *et al* [18], the EMHD flow and heat transfer of a third-grade fluid were considered. The pressure gradient term was zero in that study. The pressure gradient term was considered zero in the study of Zhang *et al* [16] also. In the present study, the pressure gradient term (dp/dx) is not zero. Moreover, the non-linear governing equations are solved by the Least Square Method (LSM), which does not require the presence of a small parameter in the problem. Consequently, the results of the present study are applicable to a wide spectrum of non-Newtonian third grade fluid parameters. Further, in the present study, the effect of cooling the flowing fluid is also included with the sign of Brinkman number (Br). As a result, both the effects of heating and cooling the fluid can be compared in the same study.

2. Problem formulation

The physical problem considered here has been sketched in figure 1. Laminar, steady, incomoressible, hydrodynamically and thermally fully developed flow conditions are assumed. The width of the plates is assumed to be very large. The properties are assumed to be constant and independent of temperature. *The* y-axis is chosen along the vertical direction; the x and z axes are along the direction of flow and lateral directions, respectively. The pressure gradient is imposed along the x-direction. An electric field is applied along the lateral ($-z$) axis and a uniform magnetic field having B as the flux density is imposed along the positive y-axis. Constant and uniform heat fluxes are supplied to both the upper and lower walls.

2.1 *Governing equations*

The flow is resulted because of the effects of externally applied pressure gradient and the electro-magnetic force

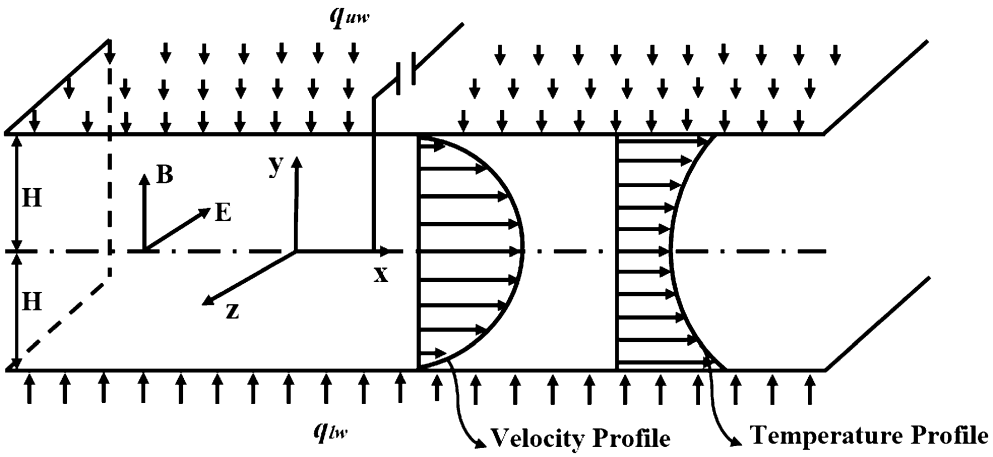

Figure 1. EMHD flow and heat transfer in parallel plates.

developed due to the interaction between the applied magnetic and electric fields. The mass conservation equation for an incompressible fluid is as follows:

$$\nabla \cdot \vec{V} = \vec{0} \tag{1}$$

where, V denotes the velocity vector. The interplay of the magnetic field and electric field gives rise to the Lorentz force, which contributes to the body force term. The conservation of momentum equation, neglecting the body force term, is given as:

$$\rho \frac{D\vec{V}}{Dt} = \nabla \cdot \underset{\sim}{\tau} + \vec{f} \tag{2}$$

where, f, τ and ρ are the body force per unit volume, stress and density respectively.

$$\vec{f} = \vec{J} \times \vec{B} \tag{3}$$

where, $\vec{f}$, $\vec{J}$, $\vec{B}$, are the body force, the current density and the magnetic field respectively. For a steady state, the left hand side of Eq. (2) reduces to zero. Under the combined influence of magnetic and electric fields, the current density is related to E and B as follows:

$$\vec{J} = \sigma(\vec{E} + \vec{V} \times \vec{B}) \tag{4}$$

where, σ is the electrical conductivity of the fluid. In the momentum conservation equation, the stress term comprises two parts; one is linear and the second is non-linear. The non-linear part, or the deviatoric stress tensor part, gives a no-linear relation between stress and strain rate for various non-Newtonian fluids. The extra stress tensor, present in the constitutive equation of a third grade fluid, is as follows:

$$\begin{aligned}\underset{\sim}{\tau} = &-p\underset{\sim}{I} + \mu\underset{\sim}{A}_1 + \alpha_1\underset{\sim}{A}_2 + \alpha_2\underset{\sim}{A}_1{}^2 + \beta_1\underset{\sim}{A}_3 + \beta_2(\underset{\sim}{A}_1\underset{\sim}{A}_2 \\ &+ \underset{\sim}{A}_2\underset{\sim}{A}_1) + \beta_3(tr\underset{\sim}{A}_1{}^2)\underset{\sim}{A}_1\end{aligned} \tag{5}$$

where, p is the static pressure, μ, α_1,α_2, β_1, β_2, β_3 are the material constants of the fluid and A_1, A_2, and A_3 represent the 1st, 2nd and 3rd Rivlin-Erickson tensors, respectively. These tensors can be obtained from the following relations:

$$\underset{\sim}{A}_1 = (grad\vec{V}) + (grad\vec{V})^{Transpose} \tag{6}$$

$$\begin{aligned}\underset{\sim}{A}_{nn} = &\frac{d\underset{\sim}{A}_{nn-1}}{dt} + \underset{\sim}{A}_{nn-1}(grad\vec{V}) + (grad\vec{V})^{Transpose}\underset{\sim}{A}_{nn-1}, nn \\ &= 1, 2, 3\end{aligned} \tag{7}$$

The rotation of the fluid element and the rate of shear strain of a fluid element are obtained by using the velocity gradient matrix $gradV^*$. Equation (5)–Eq. (7) describe the relation between shear stress and rate of shear strain using a velocity gradient vector. In Eq. (5), only up to A_1 is considered for modelling Newtonian fluids reducing the constitutive equation to linear. For non-Newtonian fluid models, however, other terms A_2 and A_3 need to be considered for capturing the non-linear behavior of the fluid.

The energy conservation equation is as follows:

$$\rho c_p \frac{D\theta}{Dt} = \underset{\sim}{\tau} : grad(\vec{V}) + \nabla \cdot (k\nabla T) + \frac{\vec{J} \cdot \vec{J}}{\sigma} \tag{8}$$

where, θ is the temperature, k is the thermal conductivity, and c_p represents the specific heat of the fluid. Under the aforementioned assumptions made in the present study, the substantial derivative in the left hand side of Eq. (8) reduces to zero. Only the axial velocity component (along the x

axis, u) exists, and it depends on y. Other velocity components along the y-axis and z-axis are zero. Consequently, the velocity vector is of the following form:

$$V = [u(y), 0, 0] \tag{9}$$

According to the assumed velocity form, as given by Eq. (9), only the u velocity component exists and upon substitution of this velocity from Eq. (9) into Eq. (2), using Eq. (3)–Eq. (7), the momentum conservation equations in the three directions are given as below:

x momentum conservation equation:

$$\frac{\partial p}{\partial x} = \mu\frac{d^2u}{dy^2} + 2(\beta_2 + \beta_3)\frac{d}{dy}\left(\frac{du}{dy}\right)^3 - \sigma B^2 u + \sigma BE \tag{10}$$

y momentum conservation equation:

$$\frac{\partial p}{\partial y} = (2\alpha_1 + \alpha_2)\frac{d}{dy}\left(\frac{du}{dy}\right)^2 \tag{11}$$

z momentum conservation equation:

$$\frac{\partial p}{\partial z} = 0 \tag{12}$$

Equation (10), Eq. (11) and Eq. (12) clearly indicate that the pressure gradient in the direction of flow is a constant. Substituting Eq. (9) into Eq. (8), the conservation of energy equation is reduced to the following form:

$$\rho c_p u\frac{\partial\theta}{\partial x} = k\left(\frac{\partial^2\theta}{\partial x^2} + \frac{\partial^2\theta}{\partial y^2}\right) + \mu\left(\frac{du}{dy}\right)^2 + 2(\beta_2 + \beta_3)\left(\frac{du}{dy}\right)^4 + \sigma(E^2 + B^2u^2 - 2EBu) \tag{13}$$

The square of the velocity gradient term in the energy equation indicates the viscous dissipation effect in the case of Newtonian fluids. In the present study, however, the fourth power of the velocity gradient term also has its share in the viscous dissipation effect. The Joule heating effects are considered by the fourth term on the right hand side of Eq. (13).

By substituting β2 and β3=0 in Eq. (13), we get the equation for the Newtonian fluid flow case. For thermally fully developed flow, the dimensionless temperature $\theta^* = \frac{\theta-\theta_{lw}}{\theta_m-\theta_{lw}}$ is a function of y^* only and is independent of x^*, where θ_m, θ_{lw} indicate the bulk mean temperature and lower wall temperature, respectively. The uniform heat flux at the boundary and the invariance of the dimensionless temperature in the axial direction result in the following equations:

$$\frac{\partial\theta}{\partial x} = \frac{d\theta_m}{dx} = const., \frac{\partial^2\theta}{\partial x^2} = 0 \tag{14}$$

Equation (14) lead to the following energy conservation equation:

$$\rho c_p u\frac{d\theta_m}{dx} = k\left(\frac{\partial^2\theta}{\partial y^2}\right) + \mu\left(\frac{du}{dy}\right)^2 + 2(\beta_2 + \beta_3)\left(\frac{du}{dy}\right)^4 + \sigma(E^2 + B^2u^2 - 2EBu) \tag{15}$$

Two boundary conditions are required for solving the second-order momentum conservation equation. These are given below as:

$$u(-H) = 0, u(H) = 0 \tag{16}$$

2.1.1 *Boundary conditions* Two boundary conditions are also required for solving energy conservation equation which are given below as:

$$k\left(\frac{\partial\theta}{\partial y}\right)_{-H} = \mp q_{lw}, k\left(\frac{\partial\theta}{\partial y}\right)_H = \pm q_{uw} \tag{17}$$

For heating conditions at the lower wall, the negative sign has to be considered as the temperature rises with a decrease in the y co-ordinate. Whereas, in Eq. (17), the positive sign needs to be considered for heating. Because with an increase in the y co-ordinate near the lower wall, the temperature rises.

2.1.2 *Non-dimensionalisation* The dimensionless temperature is modified for uniform heat flux boundary conditions using the known heat flux as follows:

$$\theta^* = \frac{\theta - \theta_{lw}}{q_{lw}H/k} \tag{18}$$

where, qlw is the imposed uniform heat flux at the lower wall. The following reference velocity and dimensionless variables are defined for reducing the momentum and energy conservation equations into their dimensionless forms:

$$u^* = \frac{u}{u_0}, y^* = \frac{y}{H}, u_0 = \frac{1}{N_1}\frac{dp}{dx}\frac{H^2}{\mu} \tag{19}$$

where, y^* and u^* are the dimensionless coordinate along the y direction and dimensionless velocity respectively. $u0$ is the reference velocity, and $N1$ indicates a dimensionless pressure gradient. Using the dimensionless variables defined by Eq. (18) and Eq. (19), the dimensionless

momentum and energy conservation equations are obtained as follows:

$$\frac{d^2u^*}{dy^{*2}} + 6A\left(\frac{du^*}{dy^*}\right)^2\frac{d^2u^*}{dy^{*2}} - \mathrm{Ha}^2u^* + H_1 = N_1 \tag{20}$$

$$\beta u^* = \frac{d^2\theta^*}{dy^{*2}} + \mathrm{Br}\left(\frac{du^*}{dy^*}\right)^2 + 2A\mathrm{Br}\left(\frac{du^*}{dy^*}\right)^4 + \mathrm{Br}Ha^2u^{*2} - \gamma_2 u^* + \gamma_3 \tag{21}$$

$$\left.\begin{aligned} A &= \frac{\beta_2+\beta_3}{\mu}\left(\frac{u_0}{H}\right)^2, \mathrm{Ha} = BH\sqrt{\frac{\sigma}{\mu}}, \mathrm{Br} = \frac{\mu u_0^2}{q_{lw}H}, \\ H_1 &= \frac{\sigma BEH^2}{\mu u_0}, \gamma_2 = \frac{EBHu_0}{q_{lw}}, \gamma_3 = \frac{\sigma E^2kH}{q_{lw}} \end{aligned}\right\} \tag{21.1}$$

where, Brinkman number Br, signifies the viscous dissipation effect, the third grade fluid parameter A signifies the intensity of non-Newtonian effect, the Hartmann number Ha implies the strength of the applied magnetic field, $H1$ implies the strength of the applied electric field compared to the viscous effect, $\gamma 2$ indicates heat generated due to the electro-magnetic interaction, and $\gamma 3$ signifies heat generated due to Joule heating. Dimensionless boundary conditions for solving the momentum conservation equation are as follows:

$$u^*(-1) = 0, u^*(1) = 0 \tag{22}$$

For solving the energy conservation equation, dimensionless boundary conditions required are as follows:

$$\theta^*(-1) = 0 \tag{22.1}$$

$$\frac{d\theta^*}{dy^*}(-1) = \mp 1 \tag{22.2}$$

$$\frac{d\theta}{dy}(1) = \pm\frac{q_{uw}}{q_{lw}} = q_r \tag{22.3}$$

Because of non-linear nature, Eq. (20) and Eq. (21), provide a challenge to obtain an exact analytical solutions. However, approximate analytical or semi-analytical solutions are possible by applying various techniques. One such method is LSM. In the present study, LSM has been employed for solving the equations. LSM does not require the existence of any small parameters. The problem is not made linear based on some simplifying assumptions. If the number of base functions or trial functions is higher, then it becomes a difficult task to find the solutions to the governing equations. Furthermore, for non-linear differential equations, a set of non-linear algebraic equations have to be solved. Another limitation is that, in most cases, LSM is employed for solving ordinary differential equations.

For further details of LSM, readers can refer to the studies conducted by the researchers [21, 24–28].

2.2 *Solution*

The first important step in solving the dimensionless momentum conservation equation, is choosing the trial functions properly. The trial functions should be chosen so that the boundary conditions are satisfied. Clearly, one of the choices for the trial functions should be of the form (1-y^{n1}) (n^1 is even). Therefore, the dimensionless velocity can be approximated by the assumed function as

$$u^*(y^*) = c_1(1 - y^{*2}) + c_2(1 - y^{*4}) \tag{23}$$

Substitution of Eq. (23) in Eq. (20) results in the generation of an error. This error can be arranged in a polynomial form as follows:

$$Rs(y^*) = a_0 + a_2y^{*2} + a_4y^{*4} + a_6y^{*6} + a_8y^{*8} \tag{24}$$

$$\begin{aligned} a_0 &= -2c_{33} - \mathrm{Ha}^2(c_{33} + c_{34}) + H - N, a_2 \\ &= -12c_{34} - 48Ac_{33}^3 + \mathrm{Ha}^2c_{33}, \\ a_4 &= -480Ac_{33}^2c_{34} + \mathrm{Ha}^2c_{34}, a_6 \\ &= 6A(32 + 12.16)c_{33}c_{34}^2, a_8 = -72.16Ac_{33}^3 \end{aligned} \tag{25}$$

Next, the square of the error has to be minimized with respect to c_1 and c_2 over the entire domain. The equations are as follows:

$$\mathrm{n}\int_{-1}^{1} Rs\frac{\partial Rs}{\partial c_{33}}dy^* = 0 \tag{25.1}$$

$$\int_{-1}^{1} Rs\frac{\partial Rs}{\partial c_{34}}dy^* = 0 \tag{25.2}$$

Solving Eq. (25.1) and Eq. (25.2) for different values of the parameters Ha, N_1, H_1 and A, c_1 and c_2 are determined. Equation (25.1) and Eq. (25.2) are coupled, non-linear algebraic equations, which are solved by using MATLAB. Substituting dimensionless velocity from Eq. (23) into Eq. (21), dimensionless energy conservation equation can be obtained and expressed in polynomial form as follows:

$$\frac{d^2\theta^*}{dy^{*2}} = b_0 + b_2 y^{*2} + b_4 y^{*4} + b_6 y^{*6} + b_8 y^{*8} + b_{10} y^{*10} + b_{12} y^{*12} \tag{26}$$

$$\left.\begin{aligned} &b_0 = \beta(c_{33}+c_{34}) - \mathrm{Ha}^2\mathrm{Br}(c_{33}+c_{34})^2 + 2\gamma_2(c_{33}+c_{34}) - \gamma_3, b_2 = -\beta c_{33} - 4\mathrm{Br}c_{34}^2 \\ &+2\mathrm{Ha}^2\mathrm{Br}c_{33}(c_0+c_{33}) - 2\gamma_2 c_{33} \\ &b_4 = -\beta c_{34} - 16\mathrm{Br}c_{33}c_{34} - 32A\mathrm{Br} - \mathrm{Ha}^2\mathrm{Br}c_{33}^2 + 2\mathrm{Ha}^2\mathrm{Br}c_{34}(c_{33}+c_{34}) - 2\gamma_2 c_{33} \\ &b_6 = -16\mathrm{Br}c_{34}^2 - 256A\mathrm{Br}c_{33}^3 c_{34} - 2\mathrm{Ha}^2\mathrm{Br}c_{33}c_{34}, b_8 = -2A\mathrm{Br}(128+1616)c_{33}^2 c_{34}^2 \\ &-\mathrm{Ha}^2\mathrm{Br}c_{34}^2 \\ &b_{10} = -1024A\mathrm{Br}c_{33}c_{34}^3 \\ &b_{12} = -512A\mathrm{Br}c_{34}^4 \end{aligned}\right\} \tag{26.1}$$

Integrating Eq. (26) twice, the dimensionless temperature is obtained, given as follows:

$$\theta^* = b_0\frac{y^{*2}}{2} + b_2\frac{y^{*4}}{12} + b_4\frac{y^{*6}}{30} + b_6\frac{y^{*8}}{56} + b_8\frac{y^{*10}}{90} + b_{10}\frac{y^{*12}}{132} + b_{12}\frac{y^{*14}}{182} + r_3 y^* + r_4 \tag{27}$$

The integration of Eq. (27) twice, leads to the generation of two constants r_3 and r_4. The third constant invoked in Eq. (27) is β (given in Eq. (21.1)), which is included in the expression for b_0. These three unknowns are evaluated by using three boundary conditions presented by Eq. (22.1)-Eq. (22.3). the bulk mean temperature θ_m is defined as

$$\theta_m = \frac{\int_{-H}^{H}\theta u dy}{\int_{-H}^{H} u dy} \tag{28}$$

The dimensionless bulk mean temperature, utilizing the dimensionless form, is expressed as

$$\theta_m^* = \frac{\theta - \theta_{lw}}{q_{lw}\frac{H}{k}} = \frac{\int_{-1}^{1}\theta^* u^* dy^*}{\int_{-1}^{1} u^* dy^*} \tag{29}$$

The Nusselt number at the lower wall is obtained as

$$\mathrm{Nu} = \frac{h_{lw}(4H)}{k} \tag{30}$$

It is already established that,

$$h_{lw}(\theta_m - \theta_{lw}) = -k\frac{\partial\theta}{\partial y}\bigg|_{y=-h} = -k\frac{q_{lw}2H}{k}\frac{d\theta^*}{dy^*}\bigg|_{y^*=-1} \tag{31}$$

$$\frac{h_{lw}(4H)}{k} = \frac{4\frac{d\theta}{dy}\Big|_{y=-1}}{\frac{\theta_m-\theta_{lw}}{(q_{lw}H/k)}} \tag{32}$$

$$\mathrm{Nu} = -\frac{4}{\theta_m^*} \tag{33}$$

2.3 *Solution for Newtonian fluids*

For validation purposes, a comparison of the results generated by LSM in the present study is made with that of the exact analytical solution of the corresponding Newtonian fluid problem. The equations governing the Newtonian fluid problem can be retraced by replacing $A = 0$ in Eqs. (20) and (21).The exact analytical solution of the dimensionless velocity is expressed as follows:

$$u^* = K_1 e^{Hay^*} + K_2 e^{-Hay^*} + \frac{H_1 - N_1}{\mathrm{Ha}^2} \tag{34}$$

where, K_1 and K_2 are obtained from the boundary conditions given by Eq. (4.22) and given as follows:

$$K_1 = K_{12} = \left(\frac{H_1 - N_1}{\mathrm{Ha}^2}\right)\left(\frac{e^{\mathrm{Ha}} - e^{-\mathrm{Ha}}}{e^{2\mathrm{Ha}} - e^{-2\mathrm{Ha}}}\right) \tag{35}$$

Substituting Eq. (34) in Eq. (21) (after the substitution of $A = 0$) we get the solution of the dimensionless temperature as follows:

$$\theta^* = \frac{l_1 e^{\mathrm{Hay}*}}{\mathrm{Ha}^2} + \frac{l_2 e^{-\mathrm{Hay}*}}{\mathrm{Ha}^2} + \frac{l_3 e^{2\mathrm{Hay}*}}{4\mathrm{Ha}^2} + \frac{l_4 e^{-2\mathrm{Hay}*}}{4\mathrm{Ha}^2} + l_5\frac{y^{*2}}{2} + K_{15}y^* + K_{16} \tag{36}$$

where,

$$l_1 = \beta c_{33} + 2\gamma_2 c_{33} - 2\mathrm{Br} c_{33}(H_1 - N_1),$$
$$l_2 = \beta c_{34} + 2\gamma_2 c_{34} - 2\mathrm{Br} c_{34}(H_1 - N_1),$$
$$l_3 = -2\mathrm{BrHa}^2 c_{33}^2, l_4 = -2\mathrm{BrHa}^2 c_{34},$$
$$l_5 = \beta \frac{(H_1 - N_1)}{\mathrm{Ha}^2} - \mathrm{Br}\frac{(H_1 - N_1)^2}{\mathrm{Ha}^2} + 2\gamma_2 \frac{(H_1 - N)^2}{\mathrm{Ha}^2} - \gamma_3 \quad (37)$$

3. Results and discussions

In this section, the flow characteristics expressed by the dimensionless velocity distribution and the thermal characteristics represented by the dimensionless temperature profiles and Nusselt number are analysed for a varying range of parameters. As the present study focuses on the EMHD transport of a third-grade fluid applied in the fields of polymer melts, rubber melts, etc., the typical values of the parameters for these applications need to be fixed first, before proceeding into the discussion of their influence on the flow and thermal characteristics. It is relevant to mention here that there is a limited availability of data regarding the physical properties of the third grade fluid in open literature.

In the study by Nayak *et al* [10], the effect of magnetic parameters (Hartmann number), Brinkman number, and third grade fluid parameters on the velocity and temperature has been analysed in the case of a wire coating problem. The present study deals with the EMHD flow and heat transfer problems of third grade fluid. Therefore, values of third grade fluid parameters are chosen in the close range as studied by Nayak *et al* [10] (0.05–0.3). In the present study, third-grade fluid parameters were chosen in the range of 0.1–0.8 [29]. Further, in the study of Nayak *et al* [10], the Brinkman number was varied in the range of 1–15. The present study also deals with EMHD flow and heat transfer of third grade fluids; third grade fluids can model polymer flow. Therefore, in the present study, Brinkman number is varied in the range of 1–5. For other parameters, the ranges chosen are close to those selected by Wang *et al* [18].

3.1 *Validation of the results*

Figure 2 represents the validation of the present study with the existing author in terms of dimensionless velocity along dimensionless coordinate in the y direction for Ha = 1, H = 3, A = 0, and A = 0.01. First, the results of Wang *et al* [18] are retraced by substituting the selected values of Ha, H, and A in Eq. (25). The resulting non-dimensional velocity distribution is then compared with that of the results reported in Wang *et al* [18]. The comparison is presented in figure 2, which exhibits excellent agreement.

In the present study, dp/dx is not considered zero. From Eq. (20) of the present study, it can be noted that if the right hand side is considered zero, then the non-dimensional momentum equations of the present study and that of Wang *et al* are the same. Therefore, for validation only, keeping other parameters the same, the right hand side is considered to be zero. As a result, the results are in good agreement.

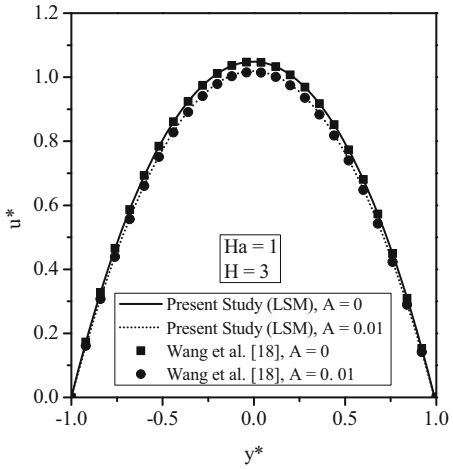

Figure 2. Comaprision of present study with existing author in terms of dimensionless velocity.

Now, if dp/dx is zero, then u_0 turns out to be zero, which should make the non-dimensional velocity infinitely large. However, this can be interpreted in the following manner: The non-dimensional velocity is a finite quantity even if dp/dx is very small, when μ is a very small quantity, or H is a very large quantity.

Therefore, for validation purposes, if dp/dx is considered as zero or a very small quantity, then u_0 is still finite provided that either μ is very small or H is a very large quantity.

Further, the results of the present investigation have been validated by comparing the dimensionless velocity and temperature distributions with the values obtained from the exact analytical solution for the Newtonian fluid flow case.

Figure 3(a) depicts the comparison of the dimensionless velocity. The comparisons of the dimensionless temperatures are presented in figure 3(b) and 3(c), which clearly reveal that the results of the present semi-analytical investigation, employing the LSM, are in excellent agreement with those of the exact solution, clearly demonstrating the suitability of the LSM for tackling the non-linear problems.

3.2 *Effect of various parameters on dimensionless velocity*

The effects of the non-Newtonian parameters *A*, Ha, and *H*1 on dimensionless velocity are depicted in figure 4(a), figure 4(b), and figure 4(c) respectively for the other parameters kept constant as given in the figure captions. Figure 4(a) clearly displays that an increase in *A* causes a

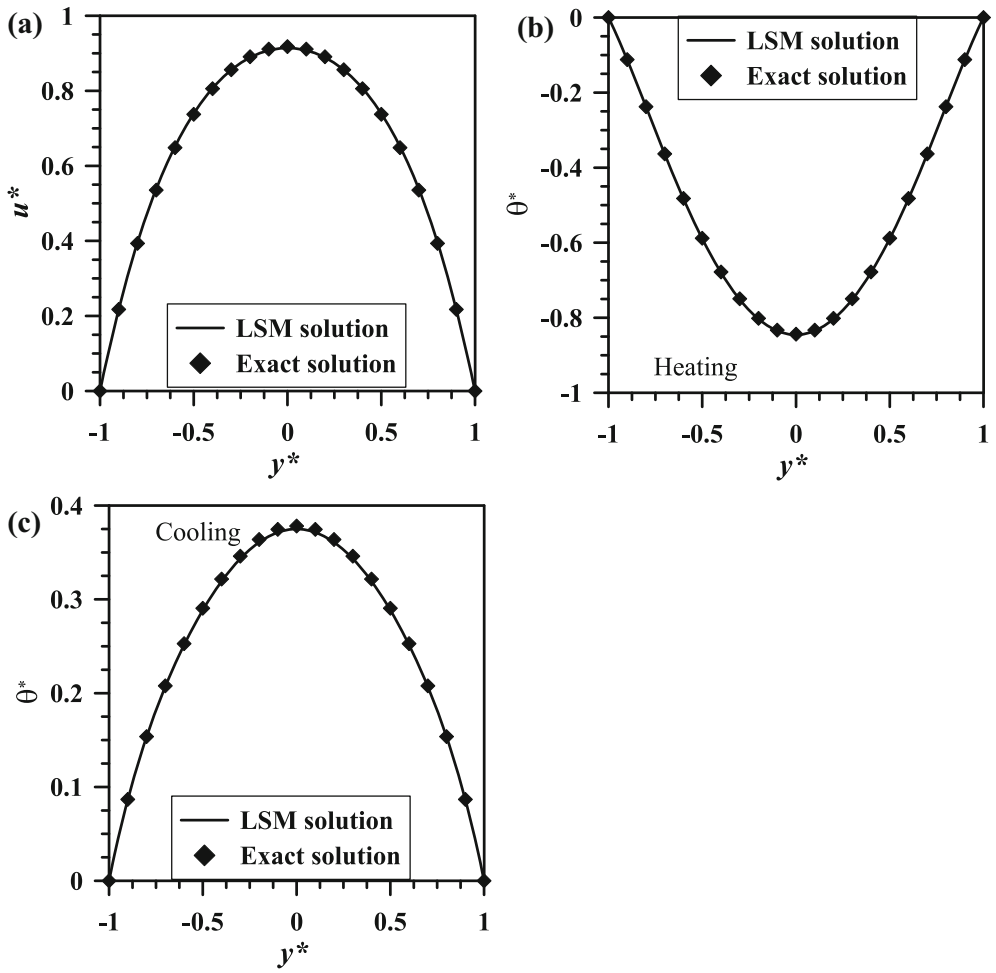

Figure 3. (**a**) Comparison between dimensionless velocity profiles (**b**) Comparison between temperature profile for cooling (**c**) Comparison between dimensionless temperature profile for cooling.

decrease in the fluid velocity. An increase in the value of A indicates an increase in the apparent viscosity of the fluid, and any increase in its value should cause a decrease in the velocity. Figure 4(b) reveals the effect of Ha on the dimensionless velocity by selecting three different values of Ha as 1, 2 and 3. As the magnitude of the externally imposed magnetic field increases, Ha increases, which causes a decrease in the velocity as the magnetic field resists the motion of the fluid. The effect of the externally applied electric field, embodied in $H1$, on the contrary, is to assist the flow, as represented in figure 4(c), by selecting three different values of $H1$ as 0.5, 1, and 2. Higher values of $H1$ result in an increase in the velocity as presented in figure 4(c).

3.3 *Effect of the various parameters on dimensionless temperature*

The influence of the imposed electrical field on temperature is displayed in figure 5(a) through a dimensionless temperature plot. The externally applied electric field, acting as an aiding force, increases the velocity, causing an increase in the convective transport of energy from one section to the other. This factor causes a decrease in bulk mean temperature and hence increases the difference between the fluid and wall temperature. The reverse happens in cooling, as depicted in figure 5(b). During cooling of the fluid, transport of more energy due to advection, because of higher velocity due to an increase in H_1, results in a decrease in bulk mean temperature. This factor results in a smaller difference between the fluid and wall temperature.

The impact of the Brinkman number on the dimensionless temperature has been displayed in figure 6(a) for heating and in figure 6(b) for cooling. During heating, an increase in the Brinkman number causes a higher viscous heating effect, causing an increase in the bulk mean temperature, which increases the difference in temperature between the fluid and the wall. The opposite trend is observed during cooling, as shown in figure 6(b). Due to the higher viscous heating as Br increases, the

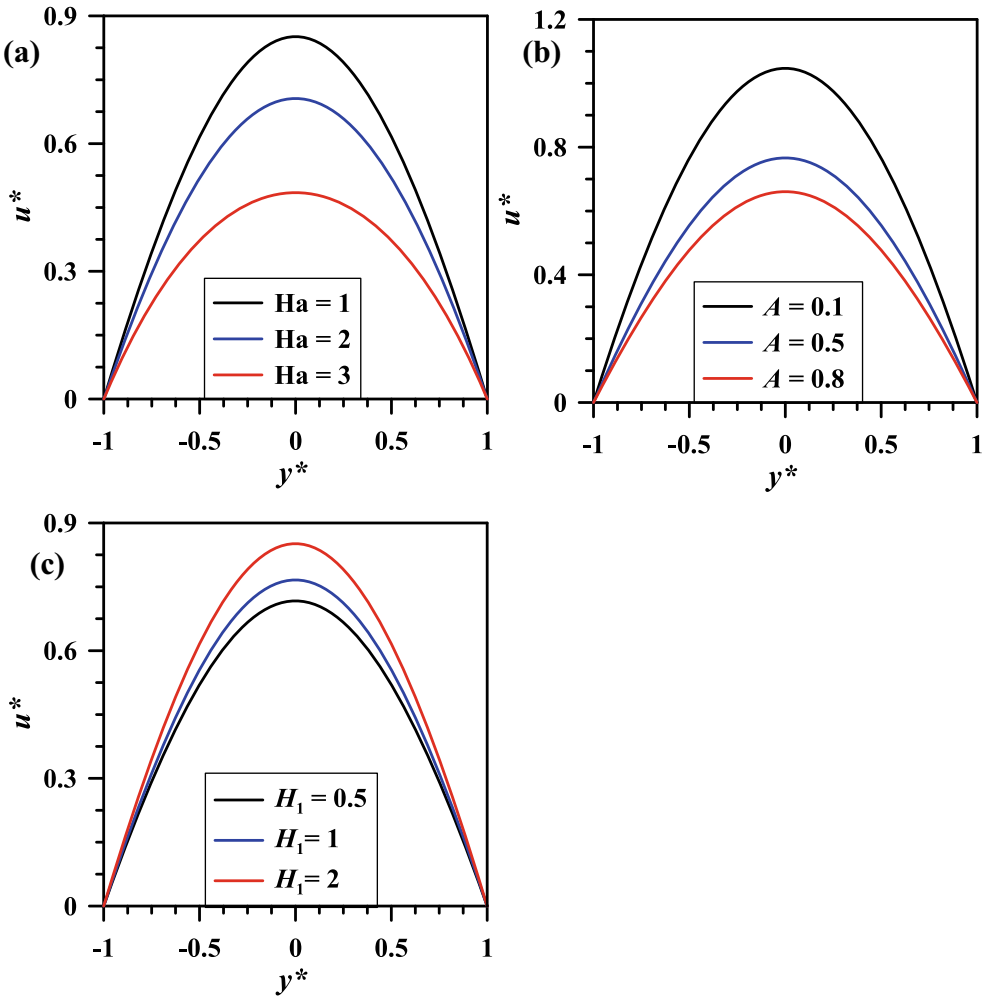

Figure 4. (**a**) Dimensionless velocity profile for different Ha when $H = 2$, $N_1 = -3$, $A = 0.4$, (**b**) Dimensionless velocity profile for different A when Ha = 2, $H = 2$, $N_1 = -3$, (**c**) Dimensionless velocity profile for different $H_1$when Ha = 2, $N_1 = -3$ and $A = 0.4$.

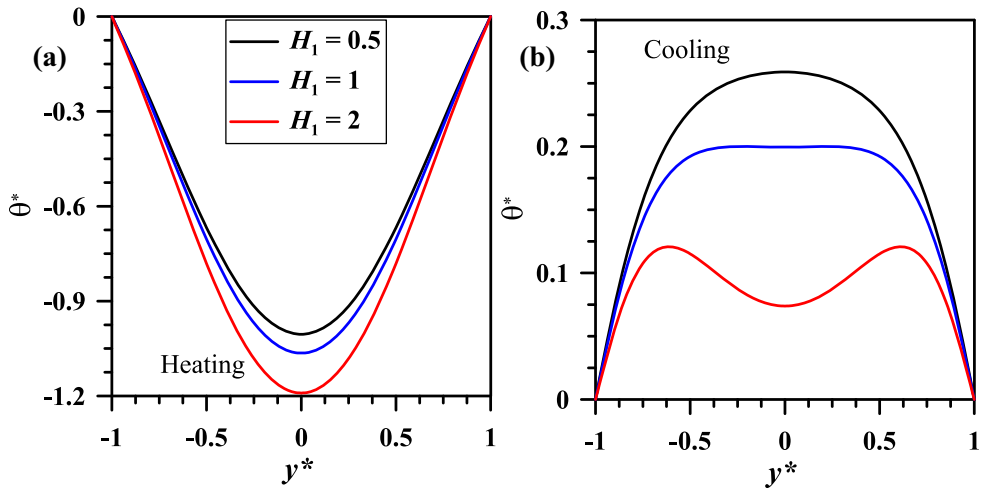

Figure 5. Dimensionless temperature profile for different H_1 when Ha = 1, $N_1 = -4$, $A = 0.4$ and $Br = 0.5$: (**a**) heating and (**b**) cooling.

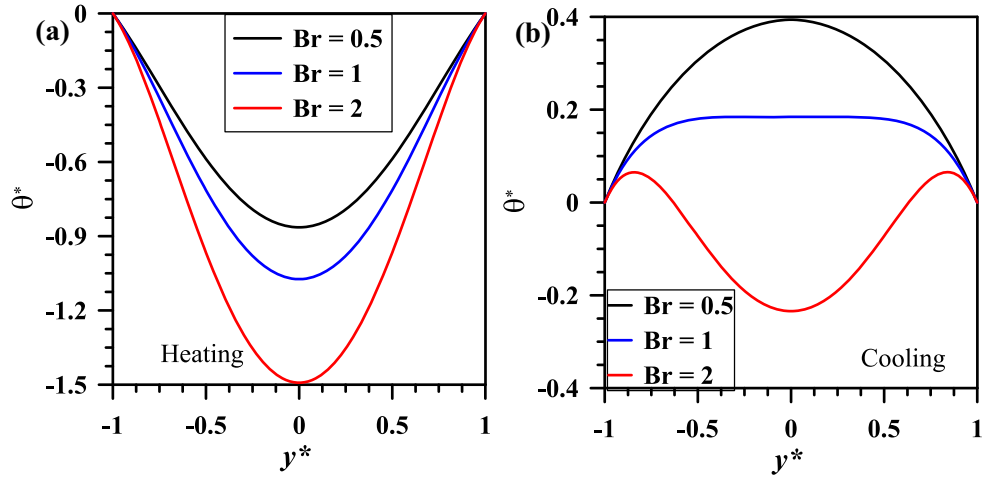

Figure 6. Dimensionless temperature distribution for various Br when Ha = 2, $H_1 = 1$, $N_1 = -4$, $A = 0.4$: (**a**) heating and (**b**) cooling.

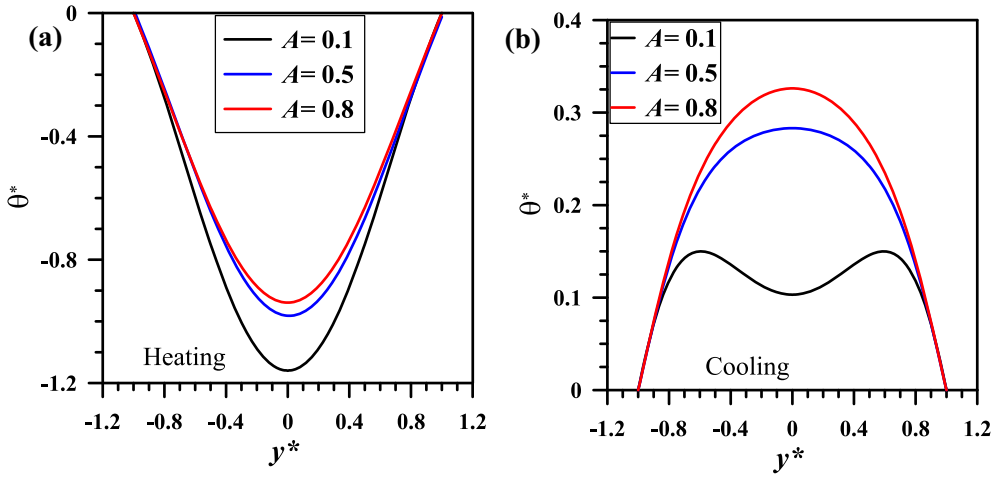

Figure 7. Dimensionless temperature profile for different A when Ha = 0.5, $H_1 = 1$, $N_1 = -3$, Br = 0.5: (**a**) heating and (**b**) cooling.

temperature of the wall also rises, as the effect of viscous dissipation is greater near the walls. Compared to this, bulk mean temperature increases marginally, reducing the difference in temperature between the fluid and the wall. It is clearly observed from the graph (figure 6(b)) that for Br=2, the dimensionless temperature of the fluid is negative beyond a certain distance from the walls, which signifies a decrease in the fluid temperature than the surface temperature while cooling (in cooling of the fluid, the wall temperature is supposed to be lower than the fluid temperature). This occurs due to a significant increase in the fluid temperature close to the wall because of the higher viscous heating effect in that region. Due to this fact, near the wall, the fluid temperature is higher, making the wall temperature also higher than the fluid temperature near the central core. In this situation, heat flows from the highest temperature region (observed as peaks very close to the wall) towards the wall and also towards the central core of the channel.

For Br greater than 2, the peak observed near the wall increases due to higher viscous dissipation. In the case of heating, for Br larger than 2, the difference between the wall and fluid increases.

Figures 7(a) and 7(b) show how the dimensionless temperature is affected by the third grade fluid parameter for heating and cooling, respectively.

Figure 7(a) indicates that the magnitude of the dimensionless temperature increases during heating with a decrease in A. As explained earlier, the fluid velocity increases with a decrease in A, resulting in a higher transport of energy by convection, causing a decrease in the bulk mean temperature of the fluid at a particular section. This factor results in a temperature difference between the wall and the fluid. In the case of cooling, the trend is the opposite, as shown in

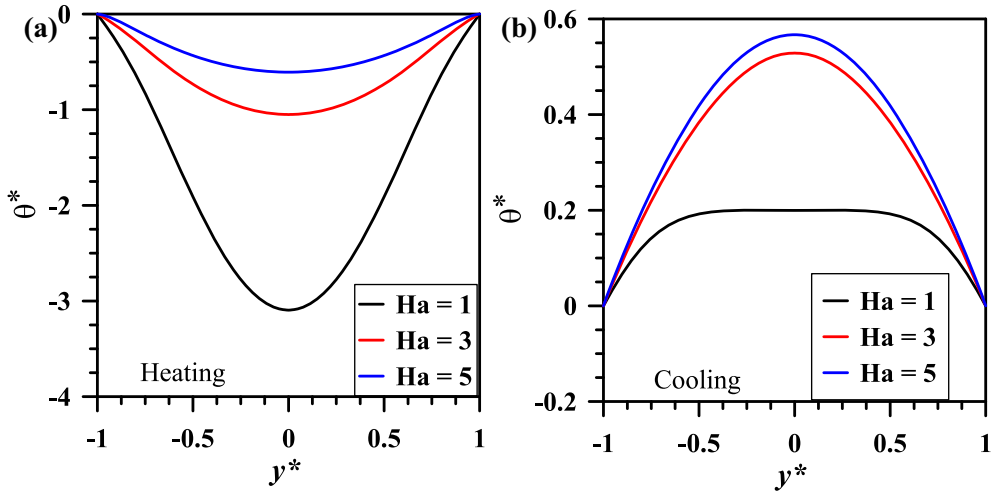

Figure 8. Dimensionless temperature profile for different *Ha* when $H_1 = 2$, $N_1 = -3$, $A = 0.3$, Br = 3: (**a**) heating and (**b**) cooling.

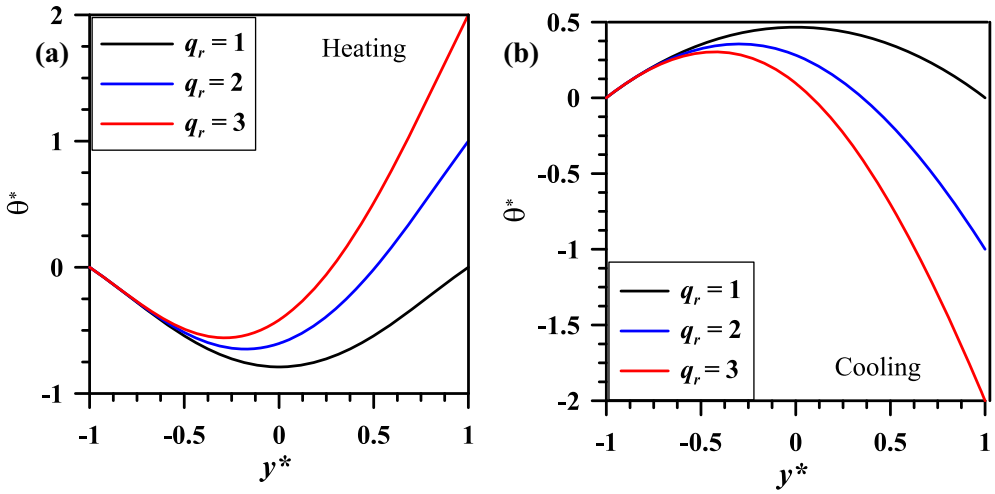

Figure 9. Dimensionless temperature profile for different H_1 when Ha = 2, $N_1 = -3$, $A = 0.5$, Br = 0.5: (**a**) heating and (**b**) cooling.

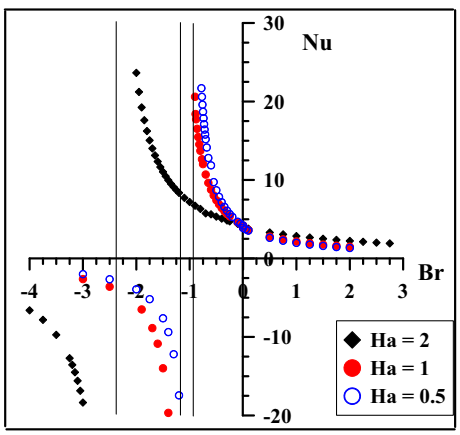

Figure 10. Variation of Nu with Br considering Haas a parameter when $H1 = 1$, $N1 = -3$ and $A = 0.4$.

figure 7(b). It is interesting to note that for $A = 0.1$, the dimensionless temperature exhibits a minimum at the centre, whereas for $A = 0.5$ and 0.8, the temperature is maximum at the centre as expected for cooling. Here, Ha = 0.5 and $H_1 = 1$ are the values of the Hartmann number and electrical strength parameter. For these values of Ha and H_1, when A is less, the opposing force on the fluid due to the applied magnetic field is comparatively less, which results in a higher velocity of the fluid and a higher transfer of energy by convection. The influence of the magnetic field is greater near the centre as the velocity increases towards the central core of the channel. Therefore, from the central part of the channel, higher energy is transported with the flow, causing a reduction in the fluid and wall temperature near the central portion. However, for Ha = 0.5 and H_1=1, velocity decreases with a rise in A, causing the

bulk mean temperature to rise and increase the difference in fluid and wall temperature.

The influence of the magnetic field, embodied in the Hartman number (Ha), on temperature is sketched pictorially in figure 8(a) for heating and figure 8(b) for cooling. The force produced by the action of the magnetic field resists the motion of the fluid, thereby decreasing the flow velocity. Due to this slowing down, the convective transport of energy is reduced, causing a temperature rise in the fluid. Due to this, the bulk mean temperature rises. The rise in bulk mean temperature causes a reduction in the fluid and wall temperature difference. An increase in Ha, therefore, results in a decrease in the temperature difference between the fluid and the wall. Figure 8(b) presents the opposite trend during cooling.

Figures 9(a) and 9(b) show the effects of changing the heat flux ratio on the dimensionless temperature. Figures indicate that a rise in the value of the heat flux ratio causes an increment in the temperature. Therefore, the dimensionless temperature of the fluid increases. During cooling, the trend is the opposite, as shown in figure 9(b).

3.4 *Effect of various parameters on Nusselt number*

The variation of Nu under the effect of Br is depicted in figure 10, considering the Hartmann number as a parameter. It is important to mention here that the negative Br can be viewed to indicate the case of cooling, so that the variation of Nu can be sketched pictorially on the same plot both for heating and cooling. Evidently, Nu decreases with increasing Br. With a rise in Br, the temperature difference between the fluid and the wall increases due to higher viscous heating close to the walls. Consequently, the difference in temperatures between the wall and the fluid increases, which indicates a decrease in heat transfer coefficient, reflected as a reduction in Nu. With an increase in Ha, Nu increases for the same Br. It is evident from the figure that Nu tends towards very large values during cooling with a decrease in the Brinkman number (the Brinkman number becomes more negative, which means a decrease numerically). However, physically, it means that for higher viscous dissipation during the cooling, the Nusselt number increases and approaches infinity asymptotically. The results indicate that the influence of Ha is to suppress this asymptotic behaviour to a large extent, as Nu approaches infinitely large values for a larger Br when Ha is high. The results indicate that Nu changes its sign for a Br (different in each case). This indicates a decrease in the bulk mean temperature to such an extent that the temperature difference between the wall and the bulk mean temperature turns out to be negative, which results in a negative value of Nu. Similar trends are reported in the investigation of Tso *et al* [27]. During this cooling, Br is so high that the viscous heating, being a maximum near the wall due to the high shear, distorts the temperature profile so that heat transfer occurs both from the near wall zone towards the wall and also from the near wall zone towards the centre line of the channel. This distortion in the temperature profile causes the bulk mean temperature to be negative. The vertical lines in figure 10 exhibit the points where the Nu changes sign.

Figures 11(a) and 11(b) show how the Nusselt number varies with the Hartmann number for different values of the third grade fluid parameter. Evidently, Nu rises with Ha for all values of A during the heating of the fluid. It is interesting to note that up to Ha = 1.75, Nu is greater for higher values of A. Flow velocity rises with a reduction in A, which causes a higher heat transfer coefficient and results in

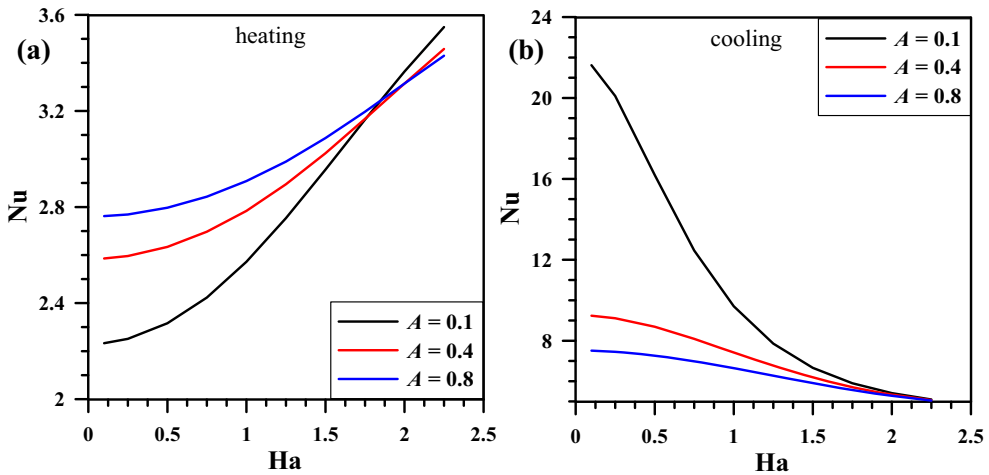

Figure 11. Variation of Nu with Ha for different when $N1 = -3$, Br = 0.5, $H1 = 1$: (**a**) heating and (**b**) cooling.

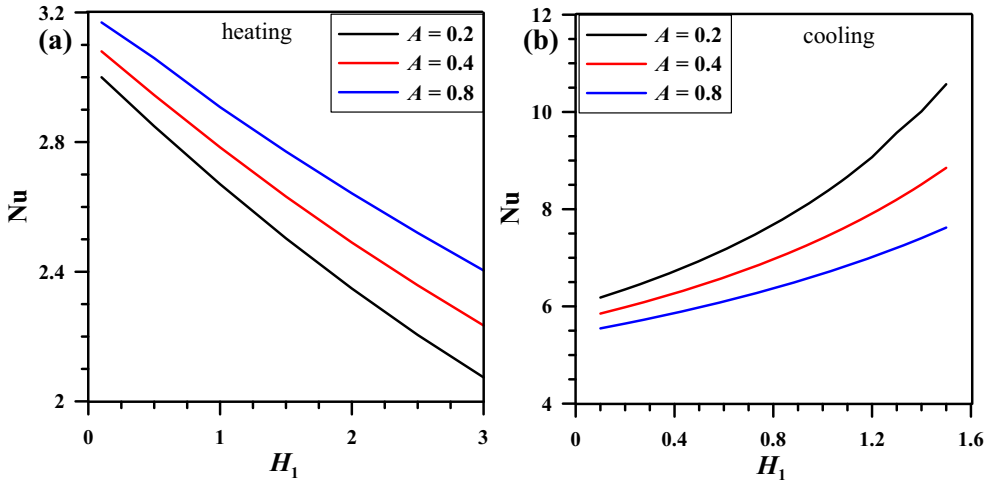

Figure 12. Variation of Nu variation with $H1$ for $N1 = -3$, Ha = 1, Br = 0.5: (**a**) for heating and (**b**) for cooling.

a higher Nu. But with a gradual increase in Ha, the opposing force on the fluid goes on increasing, and beyond Ha = 1.75, the effect of the opposing magnetic field dominates over the third grade fluid parameter's effect. That means, beyond Ha = 1.75, the velocity reduces with a rise in Ha, even if A is smaller (for smaller A, velocity should be higher). Consequently, the bulk mean temperature increases at any section, ultimately resulting in a higher Nu. In cooling, however, the reverse trend is observed, as represented in figure 11(b).

The variation of the Nusselt number with the electric field for various values of the third grade fluid parameter is shown in figure 12(a) for heating and figure 12(b) for cooling. The results indicate a decrease in the heat transfer coefficient with an increase in the value of the electric field due to the higher values of Joule heating. With an increase in the third grade fluid parameter, the velocity decreases, resulting in lower advection energy transport and thus raising the temperature at a section, which is reflected in the higher values of Nu. During cooling, the trend is reversed, as shown in figure 12(b).

4. Conclusions

The convection of third grade fluid flowing through parallel plates is investigated. Semi-analytical solutions for the velocity and temperature are obtained. The following conclusions were drawn from the study:

The results indicate that the Nusselt number reverses its sign (figure 10) when the Brinkmann number reaches a critical value. The bulk mean temperature decreases so much that the difference between the wall temperature and the bulk mean temperature becomes negative, which results in a negative Nusselt number. In the case of heating, the Nusselt number increases with the Hartmann number for all values of the third grade fluid parameter. For temperature distribution, it is observed (figure 9a) that with an increase of three times the heat flux ratio, the non-dimensional temperature rises twice in the considered range of parameters. A reverse trend is observed (figure 9b) for cooling. An increase in H_1 causes a significant increase in the velocity (figure 4c). An increase in H_1 from 0.5 to 2, in the case of heating (figure 5a), for specified values of other parameters, results in a decrease in the dimensionless temperature of around 20%. For the cooling of the fluid (figure 5b), the opposite trend is noted. An increase in Br of 0.5–2 causes the dimensionless temperature to increase (numerically) by almost 100% in the case of heating (figure 6a); an opposite trend is observed for cooling (figure 6b). For heating, the temperature difference between the fluid and the wall reduces significantly with a rise in the third grade fluid parameter.

In this study, temperature-independent properties are assumed. Temperature dependent properties can be considered for further investigation in this field, which may require the use of a mix of semi-analytical and numerical methods for solving the problem.

References

[1] Chakraborty R, Dey R and Cahraborty S 2013 Thermal characteristics of electrohydrodynamic flows in narrow channels with viscous dissipation and Joule heating under constant wall heat flux. *Int. J. Heat Mass Transf.* 67: 1151–1162

[2] Stone H A, Strook A D and Ajdari A 2004 Engineering flows in small devices microfluidics towards a lab-on-chip. *Ann. Rev. Fluid Mech.* 36: 381–411

[3] Ohono K, Tachikawa K and Manz A 2008 Microfluidics: application for analytical purposes in chemistry and biochemistry. *Electropho.* 29: 4443–4453
[4] Jang J and Lee S S 2000 Theoretical and experimental study of MHD micro pumps. *Sens. Actuat. A: Phys.* 80: 84–89
[5] Wang P J, Chang C Y and Chang M L 2004 Simulation of two-dimensional fully developed laminar flow for a magnetohydrodynamic (MHD) pump. *Biosen. Bioelect.* 20: 115–121
[6] Hoe J E 2007 Characteristics study of MHD pump with channel in rectangular ducts. *J. Mater. Sci. Tech.* 15: 315–321
[7] Rivero M and Cuevas S 2012 Analysis of the slip conditions in magneto-hydrodynamic (MHD) micro pump. *Sens. Actuat. B: Chem.* 166: 884–892
[8] Buren M, Jian Y and Chang L 2014 Electromagnetohydrodynamic (EMHD) flow through a micro channel with corrugated walls. *J. Phys. D Appl. Phys.* 47: 425501
[9] Buren M and Jian Y 2015 Electromagnetohydrodynamic (EMHD) flow between two transversely wavy microparallel plates. *Electropho.* 36: 1539–1548
[10] Nayak M K, Das G C and Singh L P 2014 Steady MHD flow and heat transfer of a third grade fluid in wire coating analysis with temperature dependent viscosity. *Int. J. Heat Mass Transf.* 79: 1087–1095
[11] Liu L C 2004 Flow and heat transfer on electrically conducting fluid of second grade over a stretching sheet subject to transverse magnetic field. *Int. J. Heat Mass Transf.* 47: 4427–4437
[12] Turkyilmaxoglu M 2012 Dual and triple solutions for MHD slip flow of non-Newtonian fluid over a shrinking surface. *Comp. Fluids.* 70: 53–58
[13] Ellahi R, Hayat T, Mohamed F M and Asghar S 2010 Effects of slip on the non-linear flows of a third grade fluid. *Nonlinear Anal. Real World Appl.* 10: 1139–1146
[14] Aziz T, Mahomed F M and Aziz A 2012 Group invariant solutions for the unsteady MHD flow of a third grade fluid in a porous medium. *Int. J. Non-Linear Mech.* 47: 792–798
[15] Li S X, Jian Y J, Xie Z Y, Liu Q S and Li F Q 2015 Rotating electro-osmotic flow of third grade fluids between two micro-parallel plates. *Colloids Surf. A: Physicochem. Eng. Asp.* 470: 240–247
[16] Zhang L, Bhatti M M and Michaelides E E 2020 Electromagnetohydrodynamic flow and heat transfer of a third-grade fluid using a Darcy-Brinkman-Forchheimer model. *Int. J. Num. Meth. Heat Fluid Flow*. https://doi.org/10.1108/HFF-09-2020-0566
[17] Hassan A R and Salawu S O 2019 Analysis of buoyancy driven flow of a reactive heat generating third grade fluid in a parallel channel having convective boundary conditions. *S N Appl. Sci.* 1(8): 919
[18] Wang L, Pongjun J, Quansheng L, Fengqin L and Cheng L 2016 Electromagnetohydrodynamic flow and heat transfer of third grade fluids between two micro-parallel plates. *Colloids Surf. A: Physicochem. Eng. Asp.* 494: 87–94
[19] Mondal P K 2014 Entropy analysis for the Couette flow of non-Newtonian fluids between asymmetrically heated parallel plates: effect of applied pressure gradient. *Physica Scripta* 89: 125003
[20] Sarma R and Mondal P K 2018 Entropy generation minimization in a pressure-driven microflow of viscoelastic fluid with slippage at the wall: Effect of conjugate heat transfer. *J. Heat Trans.* 140(5): 052402
[21] Sarma R K, Gaikwad H and Mondal P K 2017 Effect of conjugate heat transfer on entropy generation in slip-driven microflow of power law fluids. *Nanoscale Microscale Thermophys. Eng.* 21(1): 26–44
[22] Sarma R, Jain M and Mondal P K 2017 Towards the minimization of thermodynamic irreversibility in an electrically actuated microflow of a viscoelastic fluid under electrical double layer phenomenon. *Phys. Fluids.* 29(10): 103102
[23] Mondal P K and Mukherjee S 2014 Thermodynamically consistent limiting nusselt number in the viscous dissipative non-Newtonian Couette flows. *Ind. Engg. Chem. Res.* 53(1): 402–414
[24] Mahian O, Oztop H, Pop I, Mahmud S and Wongwise S 2013 Entropy generation between two vertical cylinders in the presence of MHD flow subjected to constant wall. *Int. Comm. Heat Mass Transf.* 44: 87–92
[25] Hatami M, Sheikholeslami M and Ganji D D 2014 Laminar flow and heat transfer of nanofluid between contracting and rotating discs by least square method. *Powder Techn.* 253: 769–779
[26] Hatami M and Ganji D D 2014 Thermal and flow analysis of micro channel heat sink (MCHS) cooled by cu-water nano fluid by porous media approach and least square method. *Energy Conv. Manag.* 78: 347–358
[27] Chaudhuri S and Rathore S 2019 Semi-analytical solution of the heat transfer in MHD flow of a third grade fluid. *J. Therm. Sci. Eng. App.* 11(12): 024504
[28] Chaudhuri S, Sinha S, Chakraborty P, Das M, Sahoo S and Das B 2021 Thermal characteristics of forced convection in combined pressure and shear-driven flow of a non-Newtonian third-grade fluid through parallel plates. *Heat Transf.*. https://doi.org/10.1002/htj.22201
[29] Danish M and Kumar S 2012 Exact analytical solutions for the Poiseuille and Couette-Poiseuille flow of a third grade fluid between parallel plates. *Commun. Non-Linear Sci. Num. Simul.* 17: 1089–1097